EVALUATION OF FEM-BASED MACRO-SCALE AND MICRO-SCALE THERMAL SIMULATION FOR EFFICIENT PROCESS ADAPTATION IN DIRECTED ENERGY DEPOSITION ADDITIVE MANUFACTURING

A. M. PAKDEL SEFIDI*, V. MASHETTY*, M. BEN GHORBEL*, R. OSSENBRINK*, K. SCHRICKER*

**Chair of Joining and Welding Technology, Brandenburg University of Technology Cottbus-Senftenberg, 03046 Cottbus, Germany, fg-fuegetechnik@b-tu.de*

DOI 10.3217/978-3-99161-089-2-034, license CC BY 4.0

ABSTRACT

Directed Energy Deposition (DED) involves complex thermal interactions that significantly influence microstructural properties, distortion and other final part properties. Accurate thermal modeling is essential to predict these effects and to further optimize processes. This study is motivated by the need for reliable simulation models to enable process optimization, in particular to adjust process parameters based on evolving thermal conditions. A computational framework requires efficient thermal predictions to enable adaptive control strategies, that optimize deposition parameters. This study presents a comparative analysis between two thermal modeling approaches in DED simulations: the macro-scale element clustering approach, as implemented in ANSYS DED Toolbox, and a micro-scale modeling approach based on high-resolution transient thermal simulations using the finite element method. The macro-scale simulation uses a computationally efficient approach where material is deposited in clusters and heat is applied using either a power-based or temperature-based method. While this method allows for reduced computational costs, it may lack fine-scale resolution of localized thermal gradients. On the other hand, the micro-scale FEM approach uses a mathematically defined heat source model with detailed mesh refinement and element activation, allowing for higher accuracy in capturing transient thermal effects but at the cost of increased computational requirements. While micro-scale FEM models provide accurate transient thermal analysis, their computational cost could limit their applicability for control and optimization tasks such as predictive path planning or optimized microstructures. The macro-scale simulation model offers a computationally efficient alternative, but its ability to capture relevant effects should be systematically evaluated. In this respect, the results provide a detailed insight into the relationship between computational efficiency, predictive accuracy and model applicability.

Keywords: Directed Energy Deposition (DED); Additive Manufacturing (AM); Thermal Simulation; Finite Element Method (FEM); Macro-Scale Simulation; Micro-Scale Simulation; ANSYS DED Toolbox; Wire Arc Additive Manufacturing (WAAM)

INTRODUCTION

Additive manufacturing (AM) has evolved rapidly from its origins in prototyping to the fabrication of large-scale, high-performance metallic components, with Directed Energy Deposition (DED) playing an important role in producing complex structures for the aerospace, energy, and maritime sectors [1]. This transition has intensified the demand for robust and rapid thermal simulations capable of supporting process development and component quality. Reliable thermal modeling results in the prediction of temperature fields, microstructural transformations, and residual stress distributions, offering a critical foundation for optimizing process parameters while minimizing reliance on costly empirical testing [2]. Concurrently, the integration of data-driven methodologies and the broader Industry 4.0 framework has raised the role of simulation as a key factor of both process innovation and machine learning (ML) applications in AM [3]. Recent studies have demonstrated the feasibility of training ML algorithms on simulated datasets to accurately forecast melt pool dynamics in DED, thereby facilitating real-time monitoring and adaptive control strategies [4]. This intersection of accurate physics-based simulation and data-centric techniques highlights the demand for thermal models that balance precision with computational efficiency.

One strategy to address these requirements involves the development of macro-scale thermal simulation frameworks for the Directed Energy Deposition (DED) process. Rather than resolving fine-scale and detailed melt pool simulations. In conventional thermal simulations, the heat source is often modeled using profiles like Gaussian or Goldak shapes, which were originally developed for welding [5]. Macro-scale models focus on the melt pool as an effective moving heat source and simulate heat transfer within the part using continuous thermal conduction models. This abstraction enables part-scale simulations with significantly reduced computational demands, facilitating rapid iteration over process parameters with full thermal analysis [6]. A good example is the ANSYS Additive DED Toolbox, a commercial software suite capable of simulating temperature fields, distortions, and stress evolution at the component level without modeling heat source explicitly [7]. These tools implement element activation strategies, moving heat source algorithms, and layer-by-layer thermal cycles to emulate deposition processes efficiently. In this context, Stender et al. developed a finite element-based DED workflow (applied to laser-engineered net shaping) that captured residual stresses and thermal histories with high accuracy while maintaining computational feasibility [8]. The introduction of such macro-scale models has made it possible to integrate thermal simulations into iterative process development and real-time control systems. However, these models typically apply homogenized heat input and simplified boundary conditions to accelerate computation [6]. Consequently, it becomes essential to carefully assess the predictive reliability of macro-scale approaches to Understand their capabilities and

limitations is critical when using them for process optimization or as input for data-driven methods such as machine learning.

To assess the reliability of macro-scale thermal simulations, it is important to compare them against more detailed reference data. Micro-scale models, built with finer finite element meshes, can capture steep temperature changes and variations [2]. However, their computational demands limit practical deployment in optimization processes, ML projects and large-scale simulations. In contrast, experimental thermal measurements represent the empirical information of the process and serve as necessary validation benchmarks. In DED, infrared (IR) thermography is commonly employed to monitor the evolving temperature field on the component surface throughout the build. When properly calibrated, IR cameras provide time-resolved temperature data for specific regions or layers, revealing critical thermal phenomena such as cumulative heat buildup, cooling rates, and interlayer thermal cycling. For instance, Yang et al. used calibrated IR thermography to monitor the surface temperatures during Gas Metal Arc Welding (GMAW)-based WAAM, demonstrating how variations in inter-layer dwell time directly influence heat accumulation and, consequently, part integrity [9]. Similarly, Andrade et al. conducted in-situ thermal monitoring during WAAM fabrication of 316LSi stainless steel components, establishing correlations between thermal histories and the resulting microstructural and mechanical characteristics of the deposits [10].

These studies emphasize the role of experimental thermal data in assessing the credibility of thermal simulation outputs. Consequently, by comparing macro-scale simulation results against both precise micro-scale models and experimentally acquired thermal data, we gain a much more complete picture of how accurate and useful these simplified models really are. Such comparisons help for validation and understanding the limitations of computationally efficient frameworks and provide information about their appropriate integration into process design, optimization, and control strategies.

Within this framework, the present investigation focuses on a WAAM process utilizing 316L stainless steel, with the objective of evaluating the predictive performance of a macro-scale thermal simulation model against both experimental measurements and accurate micro-scale numerical benchmarks. The deposition process involves sequential layering of 316L material using a DED system. The temporal temperature fields are captured by IR thermography. A macro-scale thermal simulation, implemented using the ANSYS AM DED Toolbox, is applied to replicate the same deposition process. This simulation employs a moving heat source model with appropriate thermal boundary conditions to estimate temperature evolution across the build without explicit modeling of melt pool. To provide a high-resolution reference, a conventional micro-scale finite element model capable of resolving steep thermal gradients and melt pool geometry is presented. The resulting temperature–time profiles from the macro-scale model are then systematically compared to the IR thermographic data and the micro-scale simulation outputs at corresponding specific location. Key thermal metrics including peak temperature, cooling rate, and pointwise comparison serve as the basis for this comparative assessment. This methodological approach is intended to investigate the central question: To what extent can a computationally efficient macro-scale DED simulation capture the thermal histories relevant for process control and optimization, and where, if at all, do significant deviations from empirical or high-fidelity reference data emerge?

SIMULATION

MACRO SIMULATION - AM DED TOOLBOX

ANSYS workbench is used to simulate the temperature field resulting from the DED process. A rectangular cuboid measuring 25*25*150 mm^3 is used for DED simulation. The model is designed with ten layers; each layer consists of five individual deposition paths. The simulation is set up in ANSYS workbench using AM DED toolbox and coupled with MATLAB to run, export and analyse the thermal data. The CAD (Computer-Aided Design) model is meshed using a Cartesian approach for the part which allows anisotropic meshing. The finer mesh used a 1.2 mm element size with stretch factors of (1, 2, 1) in X, Y, and Z directions, respectively. The coarser mesh had a 5 mm element size and stretch factors of (1, 1, 0.5) The model can be seen in Fig. 1. Respectively the entire level including weld sequence and direction is shown in Fig. 2. Unlike models that explicitly simulate the melt pool, this approach employs a macro-scale heat input method, where heat is distributed over newly activated elements rather than being resolved at a sub-melt pool level. This method, implemented in the DED AM Toolbox, allows for efficient thermal predictions while lowers computational costs. Because of this, it is reasonable to select a mesh size that fits the characteristic dimensions of the heat source without excessive refinement. Furthermore, the chosen mesh size leads to thermal predictions that closely align with experimental data, demonstrating its effectiveness in capturing essential heat transfer behaviour on the component level.

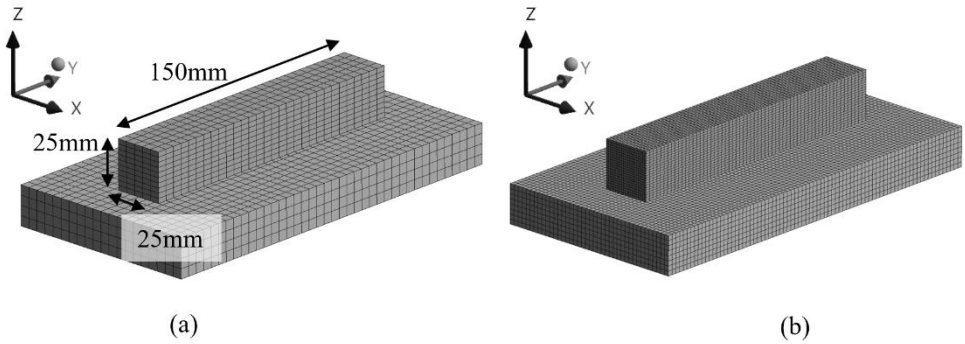

Fig. 1 The DED macro simulation model in Ansys workbench (a) 5mm mesh (b) 1.2mm mesh

In DED AM Toolbox simulation in ANSYS, the DED process is governed by a simplified thermal transient analysis, where heat is applied sequentially as new material is deposited. There are two methods to generate heat on newly activated elements: Temperature-based and power-based. In temperature-based heat generation, the temperature of activated elements is raised to the pre-set melting temperature of the material. However, in the power-based heat

generation method, a volumetric heat generation rate (HGEN) is applied to newly activated elements which considers power and absorptivity to define the heat input. The energy input for each activated cluster is calculated by the equation 1:

$$\text{Heat generation rate} = \frac{P \cdot \eta}{d \cdot t_a} \tag{1}$$

where P is power, d is deposition rate, and t_a is simulation loading applied time. η represents the process efficiency between nominal power and effective power used for deposition of the material. The heat is distributed over the volume of each cluster for a defined time span. A cluster is the set of elements which are activated at once. The simulation focuses on modelling the overall heat distribution and evolution in the part, rather than capturing detailed microstructural phenomena. For this reason, explicit modelling of the weld pool is not included. Instead, material deposition is represented by activating predefined element clusters at the material's melting temperature. Key physical phenomena such as phase transitions are incorporated via temperature-dependent material properties, included in engineering data. This approach enables efficient and accurate modelling of large-scale deposition processes without the high computational costs associated with micro-scale resolution.

Heat conduction is the primary mode of energy transfer, with additional losses occurring through convection and radiation at the exposed surfaces. Recent studies have shown that the convective heat transfer coefficient can vary significantly with temperature. For example, Tröger et al. (2024) demonstrated that during the WAAM process, the coefficient increases from around 5 W/(m²·K) at lower temperatures to values exceeding 300 W/(m²·K) as the surface becomes hotter [11]. On the other hand, Hagen et al. (2023) used a fixed value of 36 W/(m²·K) for 316L stainless steel, which provided good agreement with experimental data in their setup [12].

In Ansys DED Toolbox, it is possible to set a fixed value for the convection coefficient; however, the software also allows users to assign separate values for the base and the part, as well as for different stages of the process, the deposition phase and the subsequent cooling phase. A convection coefficient of 22 W/(m²·K) during the deposition phase and 32 W/(m²·K) during the cooling phase was set in this simulation for the base and the part. In the macro-scale model, the base plate was not explicitly included. Since the base plate acts as a major heat sink in the experiment and primarily influencing the cooling stage. The higher convection coefficient during cooling serves as an effective boundary condition to compensate for the missing thermal mass. This adjustment does not represent increased physical airflow, but restores the experimentally observed cooling rate. This combination led to the best agreement with our experimental results. Radiation losses were also included, using a calibrated emissivity value of 0.7 (see section 2.2). The material properties, including temperature-dependent thermal conductivity, specific heat capacity, and density, are integrated and can be seen in Fig. 5.

The ambient temperature is set to 23°C. The initial conditions define the starting temperature of the system, where the entire workpiece, including both the deposited material and the substrate, is set to room temperature (23°C) before deposition begins. The heat source

moves along the predefined deposition path where elements inside each cluster are activated sequentially.

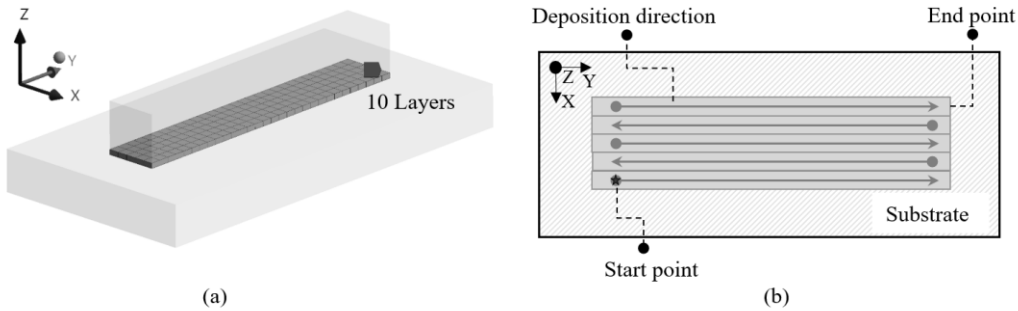

Fig. 2 (a) Macro simulation model including 10 layers; (b) Weld sequence and direction

The cluster volume represents the volume of a single deposition path, which is set in the DED AM Toolbox in ANSYS. It can be as small as a single mesh or as large as the whole weld line. The smaller the size of the cluster volume, the slower the simulation. In this study, we use the cluster volume as large as a cube 5*5*2.5 mm^3 (W × L × H) for the simulation with a larger mesh size and 1.2*2.5*1.2 mm^3 (W × L × H) for the simulation with finer mesh size. The material deposition rate (d) is derived based on the deposition speed and deposition volume per unit time. It is calculated using:

$$d = v \cdot A \tag{2}$$

where the deposition speed (v) is the travel speed of the heat source, and the cross-sectional area (A) is determined by the layer height and width of the deposited material. Each layer has a height of 2.5 mm, and the print path begins at the edge of the cube, moving from left to right and right to left in a zigzag form like which is shown in Fig. 2b. After each deposition, the power is turned off during the interpass time which is 20s.

Table 1 Simulation model parameters

Build Conditions	Value
No. of layers	10
No. of welds per layer	5
Material	316 L
Heating Method	Power based, Temperature based
Process temperature for temperature-based model	1370 °C
Heat source power for power-based model	2000 W
Process efficiency for power-based model	0.7
Gas Convection Coefficient for DED process	22 W/(m²K)
Gas Convection Coefficient for cool-down phase	32 W/(m²K)
Radiation emissivity	0.7

The total simulation time is 5300 s, reflecting the real build process, including both material deposition and cooling. The deposition phase lasts 1750 s, during which material is deposited following the predefined path. After deposition is complete, the simulation continues for another 3700 s, allowing the part to cool naturally to room temperature. Build conditions are summarized in Table 1.

MICRO SIMULATION – HEAT SOURCE MODELLED

Geometry Model

Thermo-mechanical simulations were carried out using a finite element approach in ANSYS Workbench, with user-defined APDL commands to model the WAAM process. A three-dimensional model was constructed to represent the sequential material deposition, using the Element Birth and Death technique. The geometry included both the substrate and the deposited material, which were discretized using the multi-zone meshing method available in ANSYS. This approach enables local mesh refinement in regions of high thermal gradients specifically within the weld and heat-affected zones, while allowing a coarser mesh in the

substrate to reduce computational cost. Consequently, the element edge length was set between 1.5 mm and 2.0 mm in the critical deposition regions. To model convective heat losses, a surface heat transfer coefficient of 30 W/(m²·K) was applied to all exposed surfaces of the part. Additionally, a higher coefficient of 125 W/(m²·K) was assigned to the bottom surface of the substrate, accounting for enhanced thermal dissipation due to contact with the metallic support bench. Since the exact heat transfer conditions at the interface are not precisely known, the higher value was chosen based on calibration results that demonstrated good agreement between simulation and experimental temperature profiles. Radiation losses were modelled using emissivity values of see Section 2.12. It is important to note that the applied convection settings in the micro-scale simulation differ from those used in the macro-scale model. In the macro simulation, ANSYS allows separate convection coefficients to be defined for the base and part, as well as for the deposition and cooling phases. In the micro model, a single constant convection coefficient was implemented for the entire process, which may contribute to differences observed in temperature predictions between the two approaches.

Fig. 3 illustrates the CAD geometry and mesh discretization of the finite element model, which includes both the deposition region and the substrate. The coarse mesh configuration includes approximately 11,000 elements, with dimension of 2.5*3*2.5mm (W × L × H) with an average element size of 2.7 mm in the deposited material and between 5 mm and 8 mm (averaging 6.5 mm) in the substrate. The fine mesh model consists of approximately 46,700 elements, offering higher spatial resolution with dimension of 1.66*2*1.25mm (W × L × H) with an average element size of 1.7 mm in the deposited region and about 2.7 mm in the substrate.

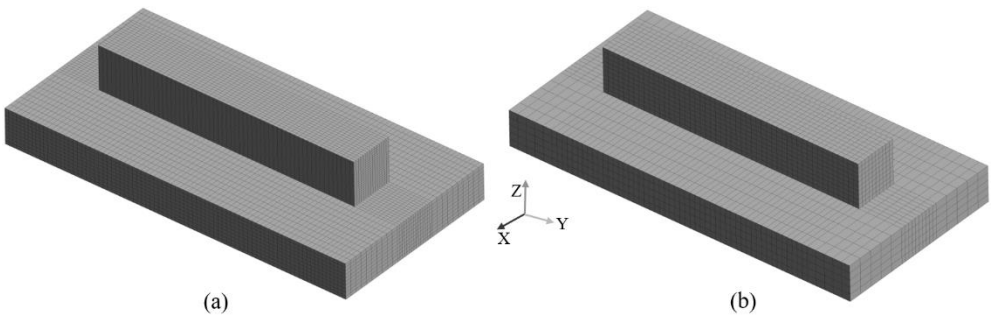

Fig. 3 Thermo-physical micro DED simulation model with detailed view of the mesh using SOLID278 elements: (a) coarse mesh with 2.75 mm element size; (b) fine mesh with 1.75 mm element size Material Deposition Modelling

This simulation model utilizes the Element Birth and Death technique to simulate the progressive deposition of material through controlled element deactivation and activation. This approach allows for staged activation of elements at predefined time steps to represent the sequential addition of material, closely mirroring the actual deposition process.

At the beginning of the simulation, all elements representing the deposited material are initialized in a deactivated (killed) state, where their thermal conductivity is reduced to a negligible value. As the simulation progresses, elements are reactivated in groups based on their position along a defined deposition path and simulation time. The progressive activation of elements is governed by a locally defined coordinate system aligned along the build direction. At each simulation time step, elements within a defined range are identified based on local coordinate system, and the corresponding elements are activated to simulate material deposition. This local coordinate system is translated incrementally along the build path, enabling continuous step-wise activation in accordance with the deposition strategy.

Using this local coordinate system, elements are selected within the following spatial range:

- X-direction (bead width): from x = –2.5 to x = 2.5 mm
- Y-direction (build path): from y = -5 to y = 5 mm
- Z-direction (layer thickness): from z = 0 to z = 2.5 mm

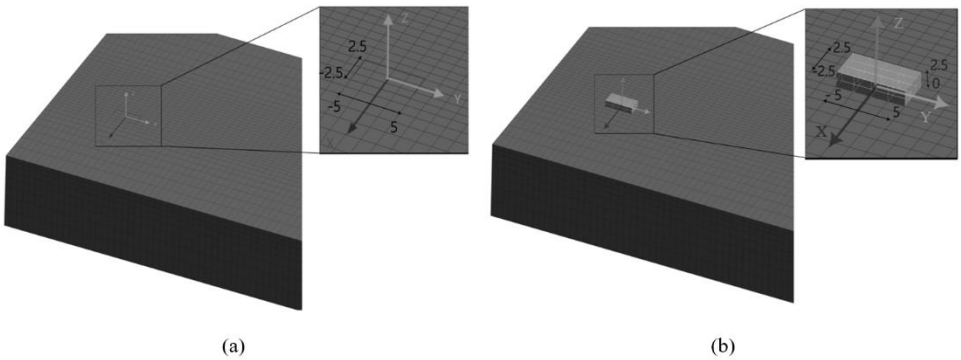

Fig. 4 Visualization of Active/Inactive Elements (a) Inactive elements (b) Active elements

Here, the x-direction represents the width of the deposited bead, while the z-direction corresponds to its height. The size of the element group within the local coordinate frame can be adjusted. For example, increasing the x-range to –5 mm to 5 mm will include a larger number of elements per set. This local activation strategy provides a high-resolution representation of material addition and heat input, in contrast to the macro-scale model, where larger clusters of elements are activated simultaneously. While the macro model approximates the thermal field over broader regions for computational efficiency, the micro model resolves finer spatial and temporal gradients, offering increased accuracy at the cost of greater computational demand.

To accurately capture the spatial variation of the Gaussian heat source, especially its exponential decay profile, it is essential to include a sufficient number of nodes along the print (build) direction. A minimum of 3 to 4 elements is typically required within this direction to avoid oversimplifying the heat input.

Time Stepping and Solution Controls

In the simulation setup, the initial time step, minimum time step, and maximum time step are all defined as 0.1 seconds. This time step setting (0.1 s) is viable for long simulations, such as 2000 seconds, balancing accuracy and computational efficiency. Reducing the time step increases computation time without necessarily improving results proportionally.

Heat Source Model

In this study, a spherical Gaussian volumetric heat source is implemented to model the thermal input during the WAAM process. This approach provides a symmetric distribution of heat around the source center and is suitable for simulating the general thermal behaviour observed during deposition [13]. The spherical Gaussian model is defined by equal semi-axes in all three spatial directions and assumes uniform heat propagation around the heat influence zone. It offers a practical balance between model accuracy and computational efficiency for capturing transient thermal fields. The volumetric heat input q is expressed as:

$$q(x, y, z) = \frac{(2 \cdot Q)}{(\sqrt{\pi^3} \cdot r_0^3)} \cdot \exp\left[- \frac{(x^2 + y^2 + z^2)}{r_0^2} \right] \tag{3}$$

$$Q = U \cdot I \cdot \eta \tag{4}$$

whereas Q is the total power input based on welding voltage U, welding current I, and thermal efficiency η, which accounts for the fraction of electrical power converted into thermal energy ($0 < \eta \leq 1$), r_0 is the effective radius of the heat source. In this study the radius of the Heat Source is 3mm and the efficiency of the Heat source is 0.8.

MATERIAL PROPERTIES

In this study, we utilized existing material properties available in the ANSYS Workbench toolbox for the DED simulation. The selected material parameters include density, specific heat capacity, thermal conductivity, and the heat transfer coefficient as temperature-dependent material properties. These properties were defined using pre-existing datasets in the ANSYS Engineering Data module for 316L stainless steel based on Kim et al. [14]. The density, thermal conductivity, and specific heat capacity as a function of temperature, allocated to both the part and the base plate, are shown in Fig. 5. According to ANSYS's official guidance, if the calculated temperature at any point exceeds the highest temperature defined in the material dataset, the software does not extrapolate further; instead, it continues to use the last defined value as constant for all higher temperatures.

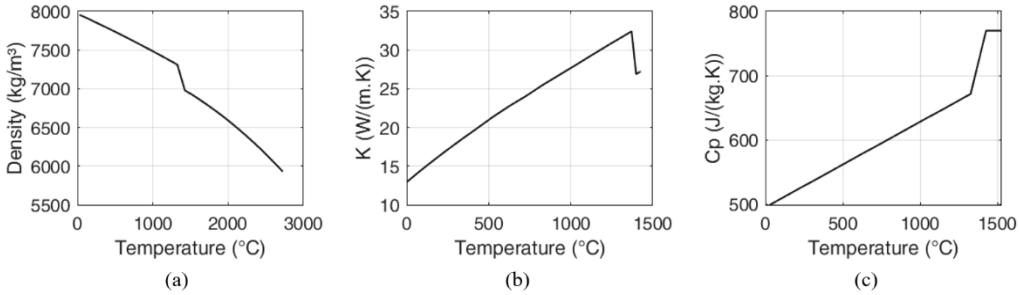

Fig. 5 Material properties as a function of temperature: (a) Density (kg/m³); (b) Isotropic thermal conductivity (W/(m · K)); (c) Specific heat at constant pressure (J/(kg · K)) [14]

CALIBRATION OF EMISSIVITY AND EXPERIMENTAL SETUP

IR THERMOGRAPHY AND EMISSIVITY IN A DED

During WAAM process, the thermal environment is highly dynamic. Temperatures range from the molten pool to much cooler surrounding material, and the surface condition evolves rapidly including developing oxides, discoloration, or soot deposits. While infrared thermography is widely used method for capturing in-situ temperature fields, its accuracy depends critically on knowing the true emissivity of the observed surface. The challenge, however, is that emissivity is neither spatially nor temporally constant. It varies with temperature, oxidation state, and even surface geometry or roughness. During WAAM, different layers and regions of the part can exhibit different emissivity values at the same time.

In practice, most IR systems require a fixed emissivity input to convert radiation data into temperature values. When this fixed value doesn't match the actual surface emissivity at a given moment, the result is an under- or over-estimation of temperature. Liu et al. (2013) demonstrated that emissivity in steel changes substantially in high-temperature environments, with oxidized surfaces showing much higher emissivity than clean or polished ones. During WAAM, recently deposited layers might exhibit low emissivity due to their reflective, molten state (typically $\varepsilon \approx 0.3–0.4$), while older, cooled layers can develop oxide films that increase emissivity well above 0.6 [15]. Similar results are shown by Hensel et al. (2024) and noted that this restriction can cause temperature fields to appear flattened or inconsistent, particularly when emissivity changes rapidly between solid and molten zones [16]. One common method is calibrating the IR camera against thermocouple readings. For example, Kindermann et al. (2023) performed WAAM thermal monitoring (in their case on Inconel 718) by embedding thermocouples in the build and adjusting the camera's emissivity until the IR-measured temperature matched the thermocouple data. They placed three K-type thermocouples at different heights within a wall and tuned the emissivity so that the IR camera's temperature readings agreed with the thermocouple measurements. This calibration

yielded an emissivity of $\varepsilon = 0.7$, which was then used for all subsequent IR measurements [17]. similarly, Farias et al. (2021) showed thermal cycles in a steel WAAM wall using an IR camera and set the emissivity to $\varepsilon \approx 0.73$ [18]. However recent DED-focused studies indicate that emissivity in the molten and near-melting temperature of 316L stainless steel is noticeably lower. In a detailed wire-laser DED investigation, Diosdado-De la Peña et al. (2025) combined infrared thermography with finite-element modelling and explicitly accounted for temperature-dependent emissivity effects [19]. Their analysis employed an emissivity of $\varepsilon = 0.21$ for the molten pool, while higher values were assigned to cooler, solidified regions. The study demonstrated that assuming higher emissivity values in the molten region leads to underestimation of peak temperatures and melt pool dimensions, supporting the use of emissivity values in the range of 0.21–0.3 for temperatures above ~1000 °C and approaching the melting point of 316L. Based on these observations, a hybrid emissivity approach is adopted in the present work. A calibrated emissivity of $\varepsilon = 0.7$ is applied in the low-to-moderate temperature ranges. At temperatures exceeding 1000 °C, emissivity values reported in the DED literature are considered.

THERMOCOUPLE-BASED EMISSIVITY CALIBRATION

In this study, we used a setup combining a reference thermocouple and the infrared camera which can be seen in Fig. 6a to calibrate the emissivity. A flat 316L plate was heated to approximately 600 °C using an oxy-fuel flame. A K-type thermocouple was attached to the surface to record the actual temperature, while the infrared camera was positioned at a distance of 100 cm. The camera's emissivity setting was then gradually adjusted until its temperature readings matched the thermocouple values during the heating and subsequent cooling phases. Throughout this process, both values were monitored in real-time. We defined an deviation margin of ±2 K between the two readings; if the difference exceeded this, the emissivity setting was further refined. Through this procedure, we arrived at a final emissivity value of 0.7, which remained consistent across the relevant temperature range. This value aligns well with emissivity ranges reported in the literature for stainless steel surfaces at elevated temperatures.

EXPERIMENTAL SETUP AND VALIDATION

To support the thermal simulation study, a physical WAAM sample was produced under repeatable process conditions. The goal was to replicate a representative deposition scenario that would allow comparison with the simulation models. The manufactured sample consists of ten layers, each composed of five parallel weld beads. The deposition sequence and movement path were programmed manually for the robot system. A solid stainless steel base plate (316L) with dimensions of 200 mm × 100 mm × 20 mm (L × W × H) was used as the substrate. A defined interpass time of 20 seconds was applied between each bead. This approach ensures reproducible thermal cycling conditions throughout the build. The deposition process was carried out in a WAAM cell. This included a KUKA KR30 industrial

robot paired with a Fronius TPS 400i power source operating in CMT (Cold Metal Transfer) mode. The filler material was 1.4430 (316LSi) stainless steel welding wire with a diameter of 1.2 mm. Shielding gas was supplied using M12 C2 (an argon-based mixture with 2 % CO_2) at a constant flow rate of 15 l/min. The contact-tip-to-workpiece distance (CTWD) was maintained within a narrow range of 12–14 mm. Fig. 6b illustrates the setup for sample fabrication, including the robot, torch, and camera arrangement. All relevant process parameters used during the experiment are listed in Table 2.

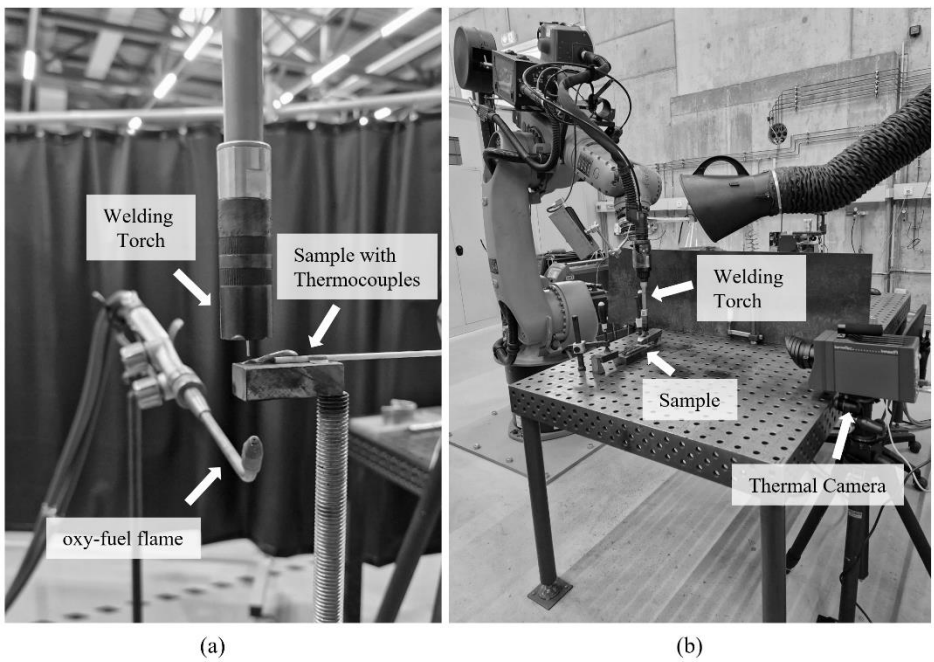

Fig. 6 Experimental setup for (a) Emissivity Calibration; (b) sample manufacturing

The Cold Metal Transfer (CMT) process was selected from the available characteristic curves provided by the Fronius TPS 400i system. The welding parameters used in the experiment are summarized in Table 2.

Table 2 The welding parameters

Wire Feed Speed, m/min	Current, A	Voltage, V	Welding speed, mm/s	Hatch Distance, mm
5.5	151	12.8	10	4

The Fronius TPS 400i system applies continuous adaptive control during the welding process. This includes real-time adjustments of current, voltage, and wire feed rate to stabilize

the arc. Prior to deposition, the substrate plate was cleaned using acetone to remove surface contaminants. After cleaning, the plate was firmly clamped onto the welding table.

An InfraTec ImageIR 8800 thermal camera, equipped with a High Dynamic Range (HDR) calibration range of 30-2000°C, was used to capture the thermal distribution for validating the simulation results. The emissivity value is set to 0.7 (see section 2.1). The HDR function in this camera extends its measurable temperature range by utilizing a fast-rotating filter wheel synchronized with the detector. This allows the camera to switch between multiple calibration settings at up to 350 Hz, combining different captured images into a single high-contrast image. The HDR function is particularly useful for monitoring high-temperature DED processes, as it enables simultaneous visualization of hot melt pool regions and cooler surrounding areas without loss of detail. This results in accurate tracking of thermal gradients, leading to a more reliable comparison between measured and simulated temperature distributions.

METHODOLOGY

DYNAMIC ERROR INDEX (DEI) FOR EVALUATING THERMAL DYNAMICS

DED processes are characterized by rapid, cyclic thermal loading, as successive layers of material are deposited and subjected to intense localized heating and subsequent cooling. Accurately capturing these transient thermal dynamics is important, because thermal gradients and cooling rates have a direct influence on microstructural evolution and induce residual stresses within the material. Conventional scalar error metrics like root-mean-square error (RMSE) or deviations in peak temperature are often insufficient for validation. A simulation may replicate the correct thermal peaks at the same time fails to accurately model the temporal effect of the heating and cooling phases. To address this limitation, it is useful to employ dynamic error measurement that quantifies differences in the rate of temperature change. These metrics, commonly referred to as dynamic error indices, that evaluates the time-derivative of the temperature signal, i.e., the heating and cooling rates rather than static values alone. The emphasis on dynamic behaviour not only ensures that a simulation aligns with thermal magnitudes, but with the complete thermal trajectory.

In this work, we introduce the Dynamic Error Index (DEI) as a measure to assess the temporal accuracy of simulated thermal histories. Because the rates at which material heats and cools play a critical role in determining phase transformations, grain structures, and residual stress patterns, incorporating temperature derivatives into validation metrics is useful.

Although macro-scale thermal models are often successful in reproducing steady-state or peak temperature values, they might fail in simulating the transient thermal behaviour. The DEI addresses this shortcoming by measuring the differences between simulated and experimental temperature derivatives, thereby providing a more sensitive and informative measure of the accuracy. This is critical as additive manufacturing systems are progressing in the sector of real-time control and machine learning-based optimization, where predictive models must accurately replicate not only thermal amplitudes but also the precise temporal

structure of temperature profiles. Building on the methodology proposed by Lázaro et al. [20], who utilized the mean absolute error of derivative curves to assess the accuracy of kinetic models in polymer decomposition, we adapt a similar framework for evaluating temperature-time histories in DED processes. In this context, we define the DEI as follows:

$$DEI = \frac{1}{N} \cdot \sum_{i=1}^{N} \left| \frac{dT_{sim}}{dt}(t_i) - \frac{dT_{\exp}}{dt}(t_i) \right| \tag{5}$$

where:

T_{sim} and T_{exp} are the simulated and experimental temperature–time curves, N is number of time steps, and t_i is each time step.

In selecting meaningful threshold values for interpreting the DEI, we considered the sensitivity of DED process to variations in heating and cooling rates. Numerous studies have shown that even small differences in thermal kinetics in the scale of a few degrees per second can significantly result in change of the microstructure, phase composition, and mechanical properties of the DED manufactured component [21]. The DEI itself measures the difference between two thermal histories, however its thresholds are motivated by experimental studies like that of Wright and Zajac (2021), who showed that even small variations in cooling rate in the range of a few K/s can lead to noticeable differences in microstructure and mechanical properties in steels [22].

Peak Temperature Error

To show local differences between simulated and experimental results we use the Peak Temperature Error (PTE). These measures help to analyze the maximum temperature reached. The PTE is defined as the difference between the maximum temperature values of the simulated and experimental curves:

$$PTE = T_{sim}^{\max} - T_{\exp}^{\max} \tag{6}$$

Peak temperature is critical as it directly influences melt pool formation and thermal gradients. It also effects directly on solidification behavior, heat-affected zones, local overheating particularly at part edges and intersections, which may cause excessive melting, vaporization, and geometric distortion. The PTE is calculated over the first five peaks, as later peaks tend to flatten, making them less sensitive for assessing simulation accuracy.

Cluster Volume in Macro Thermal Simulation

One of the key aspects investigated in this study is the effect of cluster volume on simulation accuracy and runtime. In the context of macro DED thermal simulation, cluster volumes refer to discrete blocks of material that are activated sequentially to approximate the heat input during the deposition process. Each cluster represents a portion of the deposited geometry and

the heat is applied to it when activated. The size of a cluster volume determines the dimension of heat input. Here the smaller clusters simulate the process more accurately but require more computation time, while larger clusters simplify the deposition sequence and reduce the simulation speed.

Two configurations are investigated in this study. The bigger (375 mm^3) cluster volumes and the smaller (62.5 mm^3) cluster volume. The bigger cluster volume with only five clusters per weld line. Each cluster represents roughly five times the volume of a single deposition segment. This means that instead of activating smaller regions sequentially, an entire deposition path is treated as five thermal depositions. The advantage of this approach is clear in terms of computational performance. The second configuration is the smaller cluster volume, which the entire weld line is divided into 30 clusters. Both configurations are illustrated in Fig. 7 schematically.

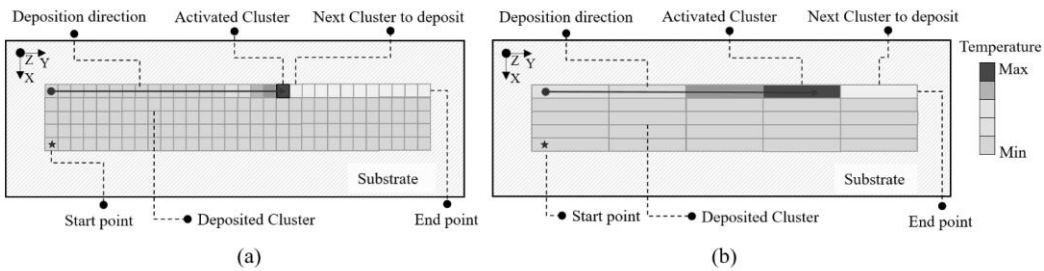

Fig. 7 Schematic illustration of clustering configurations (a) Small cluster volumes (62.5 mm^3) (b) big cluster volume (375 mm^3)

COMPARISON OF MACRO- AND MICRO-SCALE THERMAL SIMULATIONS WITH EXPERIMENTAL VALIDATION

To perform a comparative evaluation of macro-scale and micro-scale thermal simulations, both simulations are benchmarked against experimental infrared thermography. The macro-scale simulations were carried out using the ANSYS DED Toolbox, focusing on parameters such as mesh resolution, cluster volume, and heat input definition (power-based vs. temperature-based). In contrast, the micro-scale simulation was implemented in ANSYS Mechanical APDL, using a volumetric moving spherical Gaussian heat source to capture localized thermal behaviour. The temporal data for temperature is exported for a selected point as can be seen in Fig. 8 for both micro and macro simulations. P1 is the center point that is located on the top of the first layer and on the front face of the part. To assess the accuracy of micro- and macro-simulation approach, both temperature-time curves were compared directly with experimental temperature data recorded at 10 Hz during the WAAM process. The data is extracted and zoomed to the Region of interest to reduce the time of calculation. Two key metrics are used: The DEI (see section 3.1), which reflects how well the simulation captures

the rate of temperature change, and the PTE (see section 3.2), which measures how closely simulated thermal peaks align with those observed experimentally. The aim is not only to show how two simulation strategies compare to real measurements, but also how they differ from each other in terms of accuracy, computational cost, and practical usability for different kinds of analysis.

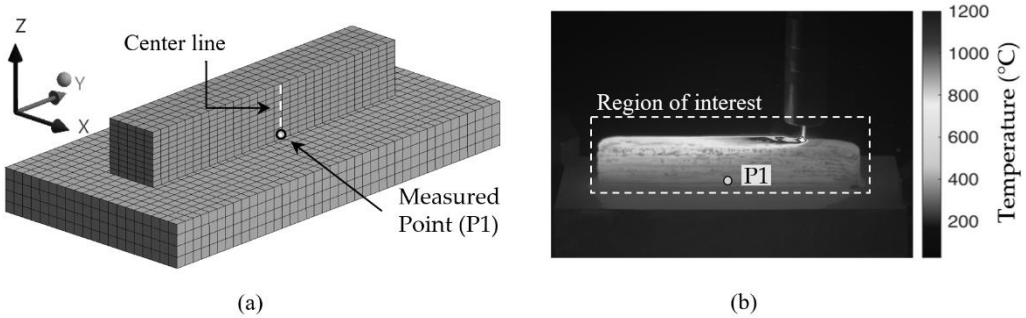

Fig. 8 Location of the selected point on (a) simulation (b) experimental thermography image

RESULT AND DISCUSSION

OVERVIEW OF MACRO AND MICRO-SCALE SIMULATIONS

Fig. 9 shows a comparative plot of performed simulations. Simulation configurations are collected in Table 3. There are three power base simulations with rough (5 mm) and finer (1.2 mm) mesh size and also small (62.5 mm^3) and bigger (375 mm^3) cluster volumes. The simulation with a temperature-based heat source is also using rough mesh and small cluster volume. Using a bigger cluster volume results in reducing simulation time dramatically, from nearly 83 minutes to 16 minutes (see Table 3), making it especially attractive for applications like trajectory optimization, where many path variations must be tested rapidly. Both configurations are illustrated in Fig. 7 schematically. However, this time-saving strategy comes with disadvantages in temperature profile prediction. Fig. 11 shows that simulations using larger cluster volumes tend to under predict temperatures, during cooling phases. This is expected, as activating a large volume all at once spreads the heat input over a broader region, smoothing out localized thermal peaks. Still, it's worth noting that the general thermal pattern including peaks and timing of peaks are preserved, indicating that even with reduced resolution, the simulation captures the overall behavior quite well. For higher-level control strategies or path planning tasks, this level of accuracy may be sufficient.

The comparison also includes a temperature-based simulation, where newly activated elements are raised directly to the material's melting point. While this method caps the peak

temperature to the process temperature and therefore can't capture overshoots the overall temperature evolution and fluctuations align closely with the power-based models.

Interestingly, even the coarser 5 mm mesh proves capable of reproducing key features of the temperature curve when used with appropriately sized clusters. This is an important observation: for simulations where fine details of the melt pool aren't the focus, and the goal is to predict thermal trends, high-resolution meshing might not be necessary. In fact, finding a balance between computational cost and predictive accuracy may be more about choosing the right cluster size than the finest possible mesh. As can be observed the finer mesh did slightly result in more accurate peak temperature predictions however the improvement over the coarse mesh case is minimal and negligible.

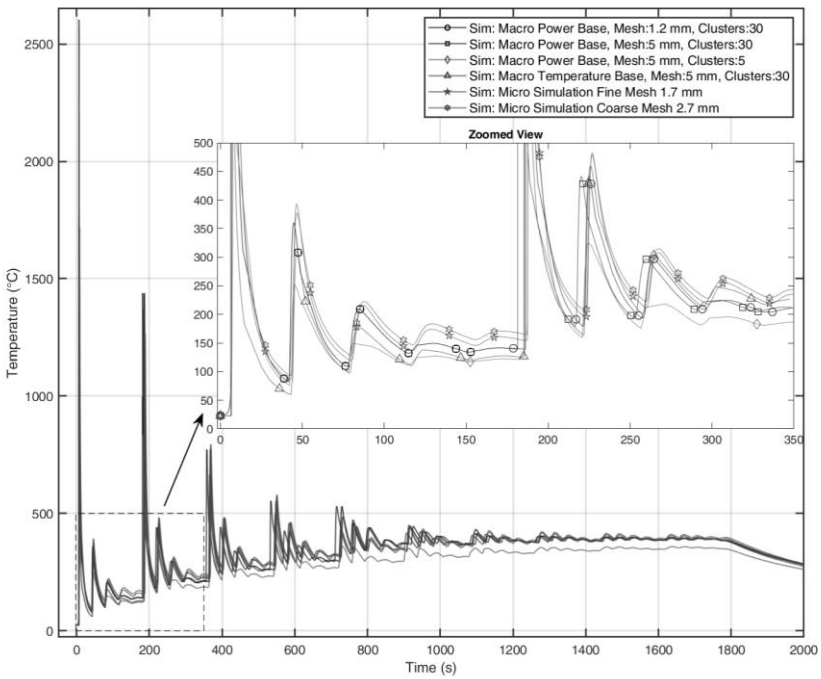

Fig. 9 Temporal comparison of performed micro and macro simulations

COMPARISON MACRO SIMULATIONS WITH EXPERIMENTAL DATA

Case 1: Macro Power-Based, Coarse Mesh (5 mm), 30 Clusters

In this case, the simulation results are compared to experimental data obtained from infrared thermography. At first glance, there's a large difference at the first peak. The simulation

predicts a temperature of around 2508 °C, while the experimental reading levels is near 1200 °C. However, this underestimation in the experimental curve is expected and can be explained by the limitations of the measurement setup. One reason to consider is that the IR camera used in this study is set to capture data at 10 Hz, which is a reasonable frame rate for thermal monitoring during WAAM. However, during rapid heating procedures, especially right after an arc burst temperature rises extremely quickly. As a result, the true thermal peak can be likely missed between frames. This adds to the deviation we see between simulation and experiment at the peaks. With this in mind, the comparison between simulation and experiment shows good agreement within the calibrated range. The simulated thermal cycles follow the experimental trend well. The timing of heating and cooling, the spacing of the peaks, and the long-term decay behavior all match closely. In the macro-scale results, a slight time shift of the later peaks was observed. This effect arises from the spatial mismatch between the experimental measurement point and the corresponding node in the coarse macro mesh. With larger element sizes and cluster volumes, the nearest simulation node can be several millimeters away from the exact thermography point, which leads to an offset in the peak positions.

The DEI curve on lower panel in Fig. 10 to Fig. 15 shows the absolute rate difference (|dT/dt|) between simulation and experiment. Spikes in this curve mostly correspond to the mismatches around thermal peaks, which as explained, are likely related to the camera resolution and emissivity issue rather than simulation error. Outside these peaks, the rate difference remains low, confirming that the simulation correctly tracks the dynamic thermal response of the process. This result suggests that even with a relatively coarse mesh, the macro-scale model performs well in capturing the essential thermal behavior, and that experimental limitations must always be considered when interpreting peak mismatches.

Two important aspects should be considered in these comparisons. First, there is a delay between the simulated and experimental temperature peaks, particularly in the later stages of the process in some cases. This misalignment is due to the coarse mesh resolution, which limits the ability to select a simulation point that precisely matches the experimental measurement location. As the elements are large, the selected point may lie offset from the actual experimental measurement point, leading to small shifts in peak timing. In the lower panel showing the DEI, many red segments appear as flattened lines. DEI values greater than 10 K/s are considered poor agreement, and are therefore visually capped to preserve the resolution and readability of more relevant regions where DEI is below 10. DEI values less than 5 K/s is shown in green, and DEI values in the 5-10 K/s range is shown in blue.

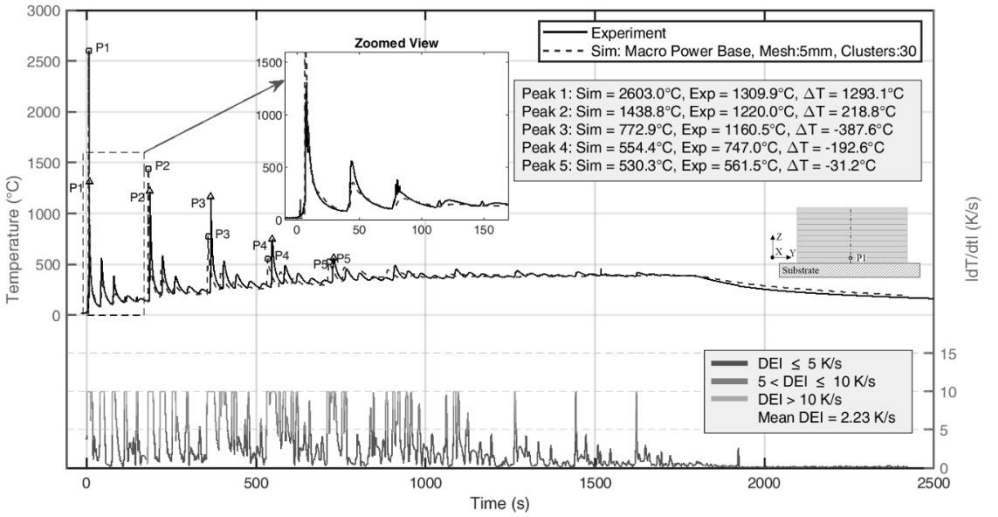

Fig. 10 Result comparison between experimental data and macro simulation: Power-based, 5mm Mesh (coarse mesh), 30 clusters per weld line (small cluster volume)

Case 2: Macro Power-Based, Coarse Mesh (5 mm), 5 Clusters (large cluster volume)

In this case, the simulation was performed using only 5 clusters per weld line, which means each cluster covers a volume about five times larger than that of a typical single deposition segment. Rather than simulating the path of the moving heat source in fine steps, the entire deposition line is activated in larger portions. This extremely reduces computational time by over 80% compared to the standard 30-cluster setup. As shown in Fig. 11, the simulated temperature curve is shifted downward compared to the experimental data. While the number and timing of peaks are captured fairly correct, the peak values themselves are underestimated slightly compared to finer cluster volumes, especially beyond the second peak. This is expected as larger clusters distribute the heat over a bigger volume all at once, which smooths out sharp thermal gradients and reduces the intensity of local heating. However, the overall thermal behavior is preserved. The DEI in this case is higher than in the 30-cluster version (3.2 K/s vs. 2.27 K/s).

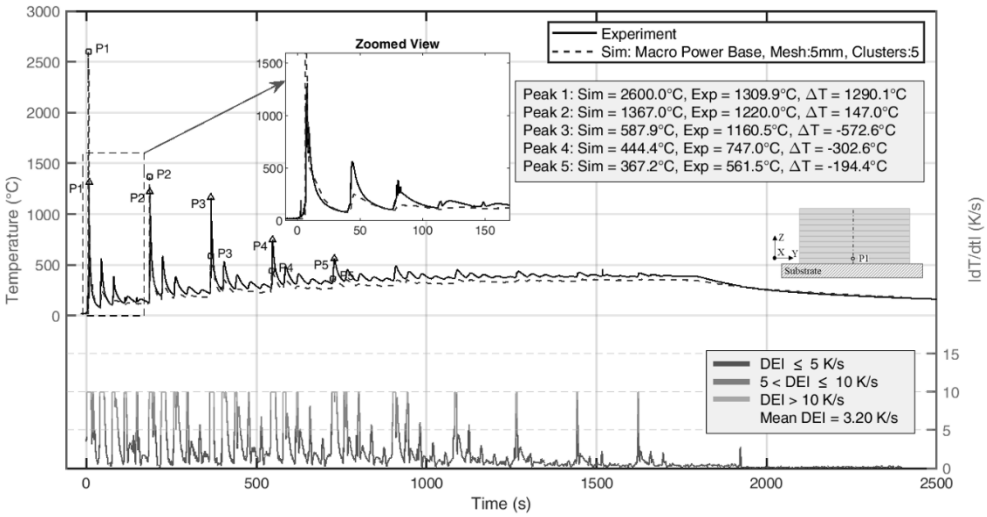

Fig. 11 Result comparison between experimental data and macro simulation: Power-based, 5mm Mesh (Coarse mesh), 5 clusters per weld line (Coarse cluster volume)

Case 3: Macro Temperature-Based, Coarse Mesh (5 mm), 30 Clusters (small cluster volume)

This simulation was performed using the temperature-based heat input model. In this model, each cluster is simply brought up to the material's preset melting temperature (1370°C) the moment it's activated. What's immediately noticeable is that this case result in lower mean DEI of 2.05 K/s, which tells us the simulation tracks the rate of heating and cooling quite well. The alignment of temperature-time curve with experimental data is actually very good (see Fig. 12), particularly in terms of how the temperature rises and falls through each layer cycle. The fluctuations are captured clearly, and the timing of thermal cycles matches nicely.

As mentioned, the method also puts a cap on the peak temperatures, since it forces each cluster to the melting point and no higher. While the overall shape of the curve looks realistic, we don't see the same high peak temperatures that are common in real processes, especially at the start of the process. So in that sense, we lose the ability to model thermal overshoots or localized overheating, which can be important depending on the application. The simulation run time is exactly the same as the power-based model with the same mesh and cluster setup, about 1 hour and 23 minutes.

If the focus of the study is mainly on temperature trends, layer-wise thermal cycles, or relative comparisons, this temperature-based model is probably good enough. But if the focus of the investigation is on cooling rates, or phase changes, then it is logical to use the power-based approach, since it gives a better prediction on actual thermal changes.

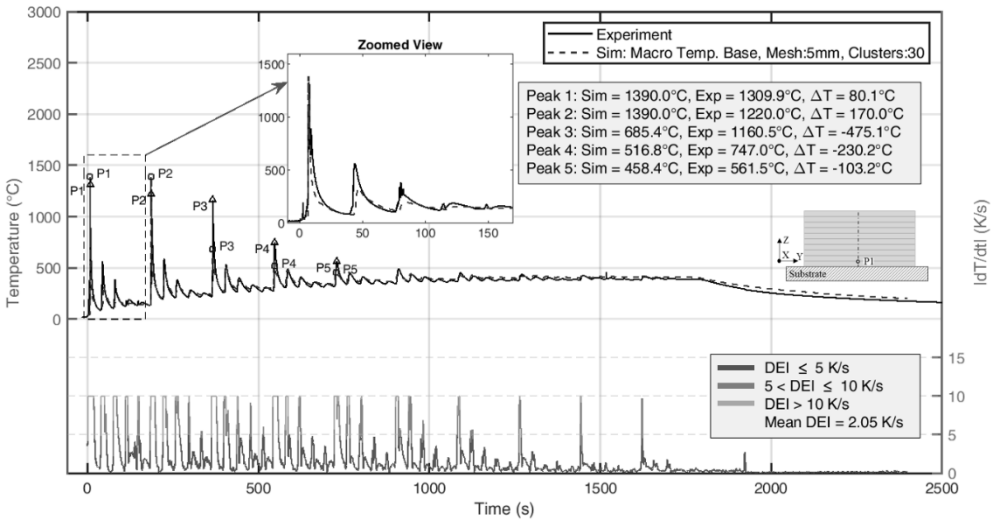

Fig. 12 Result comparison between experimental data and macro simulation: Temperature-based, 5mm Mesh (coarse mesh), 30 clusters per weld line (small cluster volume)

Case 4: Macro Power-Based, Fine Mesh (1.2 mm), 30 Clusters (small cluster volume)

This case uses a fine mesh 1.2 mm for the part and 2.5 mm for the base, while keeping the number of clusters at 30, like in previous runs. This results in the best overall match with the experimental data. The DEI drops to 1.98 K/s, which means the model is closely following the way temperature changes over time. The simulation aligns well with the experiment, especially in the later stages (see Fig. 13). The peaks are located in time, and the changes are quite well captured. Peak 5 which in earlier cases had a bigger offset, now comes closer, with a difference of just about 32.7 °C. So in terms of overall trend and accuracy, this model performs the best. The simulation took over 19 hours to run, which is ten times longer than the coarse-mesh cases. That's a serious computational cost, and it means this approach isn't very practical if you need to run many simulations, like in optimization studies. For cases where thermal history needs to be as realistic as possible, the fine mesh does its job. Still, there's room to improve performance. For example, using multi-zone meshing for substrate, where high resolution is used only around the contact to the part and coarse elements are used elsewhere, could reduce runtime while keeping the accuracy where it matters.

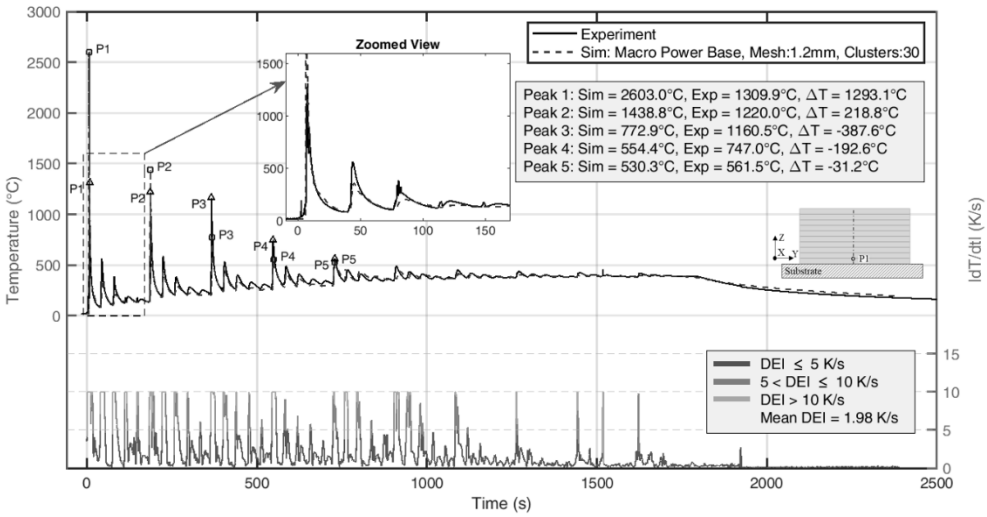

Fig. 13 Result comparison between experimental data and macro simulation: Power-based, fine mesh 1.2mm, 30 clusters per weld line (small cluster volume)

COMPARISON OF MICRO SIMULATIONS WITH EXPERIMENTAL DATA

Case 1: Micro Power-Based, Fine Mesh (1.2 mm), spherical Gaussian heat source

Fig. 14 shows the temperature history, comparing experimental data with the micro-scale simulation using a fine mesh resolution of 1.7 mm in average. The simulation captures the transient temperature evolution in good agreement with the experiment. The DEI shown in the lower plot, remains low throughout the process, with the majority of values below 5 K/s (green), fewer in the 5 - 10 K/s range (blue), and some instances exceeding 10 K/s (red) which are mostly related to peaks. The mean DEI is 1.91 K/s, which is lower than the macro-scale models, indicating a more accurate temporal evolution. The enlargement on the initial segment highlights the simulation's ability to follow the sharp gradients at early peaks. The PTE is also evaluated for each peak and summarized in the inset. As discussed previously, the absolute differences are influenced by factors such as emissivity settings, rather than simple over- or underestimation by the model (see section 4.2.1). Compared to the macro-scale simulations, the micro-model with fine mesh shows an improvement in both peak alignment and temporal accuracy.

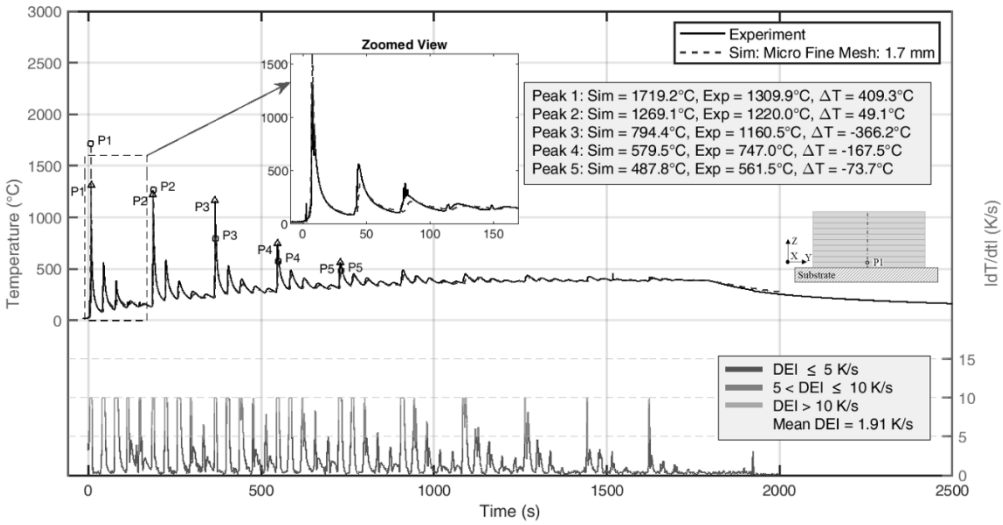

Fig. 14 Result comparison between experimental data and micro simulation: 1.7mm Mesh (fine mesh), Gaussian heat source

Case 2: Micro Power-Based, Coarse Mesh (2.7 mm), spherical Gaussian heat

Fig. 15 presents the thermal history for the micro-scale simulation using a coarser mesh resolution of 2.7 mm. The overall temperature evolution closely follows the experimental trend, with six distinct peaks. The temporal agreement remains strong, as evidenced by the DEI plot at the bottom, where most values remain below 5 K/s, with some moderate deviations and a few high-error events during rapid thermal cycles. The mean DEI is 1.95 K/s, nearly identical to the fine mesh case, suggesting that coarsening the mesh does not significantly weaken the temporal accuracy of the simulation. A zoomed view of the early stage confirms that the simulation reproduces the steep gradients well, however with less detail in the peak curvature. The PTE remains consistent with earlier observations, with lower accuracy at early peaks, while later peaks align more closely. Compared to the fine mesh result, this setup offers a comparable DEI but with a reduced computational cost, making it a potentially more efficient option where precise spatial gradients are less needed.

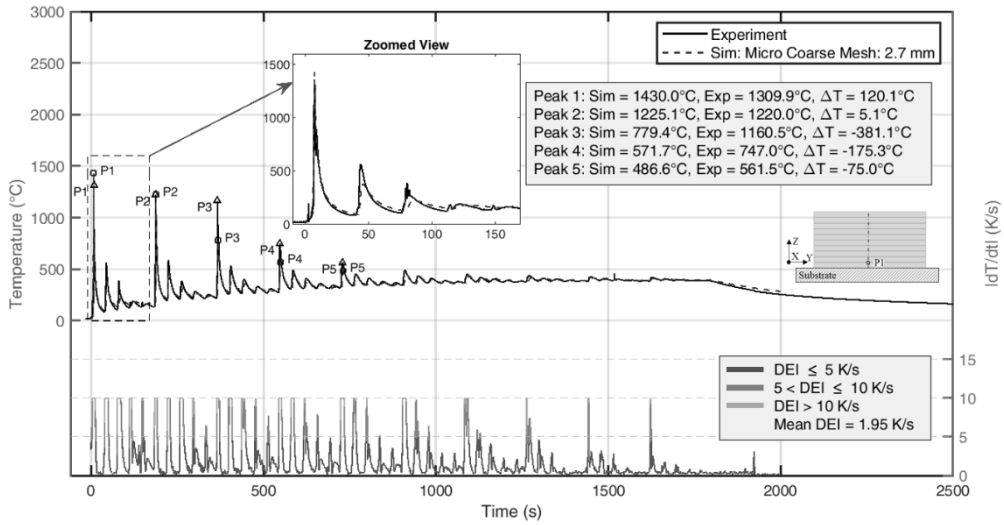

Fig. 15 Result comparison between experimental data and micro simulation: 2.7mm Mesh (coarse mesh), Gaussian heat source

DISCUSSION AND IMPLICATIONS

Table 3 provides an overview of all simulation cases. It compares macro and micro models with respect to mesh size, heat source type, number of elements, cluster volume, simulation time, and resulting DEI values. Among the macro simulations, the finest mesh setup (1.2 - 2.5 mm) with a power-based heat source achieves a low DEI of 1.98 K/s, but at the cost of a significantly long simulation run time of over 19 hours. In contrast, using a coarser mesh (5 - 5 mm) considerably reduces the runtime to 1.5 hours, but increases the DEI to 2.23 K/s, showing the trade-off between efficiency and accuracy. The same coarse mesh, when applied with a higher cluster volume (375 mm^3) and fewer clusters per weld line, further reduces runtime to just 16 minutes, but leads to the highest DEI of 3.2 K/s, indicating clear accuracy reduction of the simplified model. The macro model with temperature-based input maintains a runtime similar to the power-based version (1 hour 23 min) but with a slightly improved DEI of 2.05 K/s, suggesting better temporal agreement with existing experimental results. The best DEI of 1.95 K/s for the coarse mesh and 1.91 K/s for the fine mesh belong to two micro simulations, both using spherical Gaussian heat source while maintaining higher computational cost. The coarse mesh model runs in 3:40 hours, and the fine one in 9:57 hours. They offer a more advantageous balance between accuracy and runtime than the high-resolution macro simulation. The results clearly show that while macro models are performing well for capturing the heat distribution, micro-models provide better accuracy in capturing local thermal changes, especially when carefully meshed and fed with realistic boundary conditions.

Table 3 Summary of simulation parameters and results

Sim. type	Heat Source type	Mesh size part-base mm	No. of Elements	Cluster Volume mm^3	Clusters per weld line	Run time h:min	DEI K/s
Macro	Power Based	1.2-2.5	52181	62.5	30	19:18	1.98
Macro	Power Based	5-5	4700	62.5	30	01:23	2.23
Macro	Power Based	5-5	4700	375	5	00:16	3.2
Macro	Temperature based	5-5	4700	62.5	30	01:23	2.05
Micro	Gaussian	2.7-6.5	11000	125	28	3:40	1.95
Micro	Gaussian	1.7-2.7	46700	125	28	9:57	1.91

Fig. 16 visualizes the relationship between simulation time and temporal accuracy (expressed by DEI) for all studied cases. The overall trend highlights a clear clustering: micro simulations (Sim 5 and Sim 6) achieve the lowest DEI while having higher computational cost, positioned in the lower-mid region of the plot. In contrast, the most accurate macro model (Sim 1) requires over 20 hours to reach a similar DEI level. Notably, Sim 3 with minimal simulation time, exhibits the poorest accuracy, confirming that excessive simplification leads to temporal deviation. Sim 2 and Sim 4, both macro models with identical mesh but differing heat input strategies, show comparable runtime but slightly different DEI outcomes. The results show that while macro models correctly capture the overall heat flow in the entire part, micro models are more suitable for detailed thermal analysis in specific regions. Although both approaches can achieve similar accuracy in terms of DEI, except for the macro model with very large cluster volume.

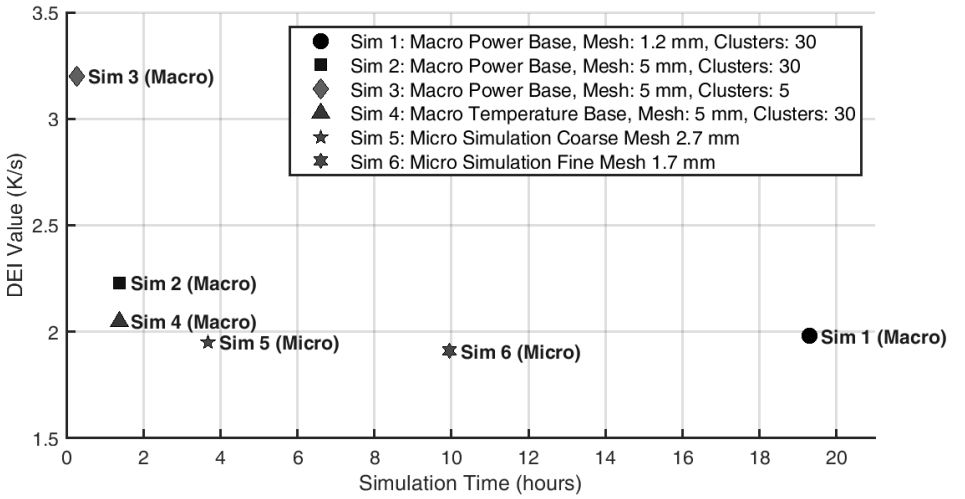

Fig. 16 DEI plotted against simulation time for six simulations, labeled by type and configuration

SUMMARY AND OUTLOOK

This study presented a multiscale simulation framework for predicting the thermal history in WAAM of 316 L stainless steel, combining macro modelling for power-based and temperature-based heat propagation with micro heat source modelled simulations. Experimental validation using thermal camera measurements enabled an assessment of various modelling strategies in terms of temporal accuracy and computational efficiency. The Dynamic Error Index (DEI) and Peak Temperature Error (PTE) were introduced as evaluation metrics, revealing that finely meshed micro models deliver the best agreement with experimental data while maintaining higher runtime. In contrast, the macro models, particularly those with fewer clusters or coarser meshes, showed some loss in accuracy. However, the overall results demonstrate that macro-scale simulations can still deliver acceptable accuracy with lower computational costs. This makes them attractive for applications where large numbers of simulations are needed, such as in optimization loops or machine learning-based models used for real-time process control or adjustments. For instance, in studies aiming to adjust deposition strategies in DED to achieve targeted temperature profiles, fast-running macro models offer a practical solution.

ACKNOWLEDGMENT:

This project on which this publication is based was funded by the federal Ministry of Education and Research under the funding code 02P21Z000.

References

[1] A. RIENSCHE, J. SEVERSON, R. YAVARI, N. L. PIERCY, K. D. COLE and P. RAO: 'Thermal modeling of directed energy deposition additive manufacturing using graph theory', *Rapid Prototyping Journal*, Vol. 29, No. 2, pp. 324-343, 2023.

[2] P. S. COOK and A. B. MURPHY: 'Simulation of melt pool behavior during additive manufacturing: Underlying physics and progress', *Additive Manufacturing*, Vol. 31, p. 100909, 2020.

[3] Z. ZHANG, Z. LIU and D. WU: 'Prediction of melt pool temperature in directed energy deposition using machine learning', *Additive Manufacturing*, Vol. 37, p. 101692, 2021.

[4] M. M. IMRAN ET AL.: 'Prediction of melt pool height based on the spatiotemporal adjacency features in laser metal deposition using machine learning', *Progress in Additive Manufacturing*, 2025.

[5] J. CHENG, Y. HUO, P. FERNANDEZ-ZELAIA, X. HU, M. LI and X. SUN: 'A Gaussian Process-Based extended Goldak heat source model for finite element simulation of laser powder bed fusion additive manufacturing process', *Computational Materials Science*, Vol. 244, p. 113185, 2024.

[6] R. F. V. SAMPAIO, J. P. M. PRAGANA, I. M. F. BRAGANÇA, C. M. A. SILVA, C. V. NIELSEN and P. A. F. MARTINS: 'Modelling of wire-arc additive manufacturing – A review', *Advances in Industrial and Manufacturing Engineering*, Vol. 6, p. 100121, 2023.

[7] ANSYS INC.: *Additive Manufacturing & 3D Printing Simulation Software (Directed Energy Deposition)*, Ansys Product Brochure, 2021.

[8] M. E. STENDER ET AL.: 'A thermal-mechanical finite element workflow for directed energy deposition additive manufacturing process modeling', *Additive Manufacturing*, Vol. 21, pp. 556-566, 2018.

[9] D. YANG, G. WANG and G. ZHANG: 'Thermal analysis for single-pass multi-layer GMAW based additive manufacturing using infrared thermography', *Journal of Materials Processing Technology*, Vol. 244, pp. 215-224, 2017.

[10] D. G. ANDRADE, T. TANKOVA, C. ZHU, R. BRANCO, L. S. DA SILVA and D. M. RODRIGUES: 'Mechanical properties of 3D printed CMT-WAAM 316 LSi stainless steel walls', *Journal of Constructional Steel Research*, Vol. 215, p. 108527, 2024.

[11] J.-A. TRÖGER, S. HARTMANN, K. TREUTLER, A. POTSCHKA and V. WESLING: 'Simulation-based process parameter optimization for wire arc additive manufacturing', *Progress in Additive Manufacturing*, Vol. 10, No. 1, pp. 1-14, 2025.

[12] L. HAGEN ET AL.: 'High deposition rate wire-arc directed energy deposition of 316L and 316LSi: Process exploration and modelling', *Materials Science and Engineering: A*, Vol. 880, p. 145044, 2023.

[13] V. MICHAILOV, N. DOYNOV and R. OSSENBRINK: *Sensibilitätsanalyse der thermomechanischen FE-Schweißsimulation*, Shaker Verlag, May 2012, ISBN: 978-3-8440-1016-9.

[14] C. S. KIM: *Thermophysical properties of stainless steels*, Argonne National Laboratory (ANL), Argonne, IL (United States), 1975.

[15] Y. F. LIU, Z. L. HU, D. H. SHI and K. YU: 'Experimental investigation of emissivity of steel', *International Journal of Thermophysics*, Vol. 34, No. 3, pp. 496-506, 2013.

[16] J. MÜLLER and J. HENSEL: 'Potential of thermography for the monitoring of DED-Arc processes', *Weld World*, Vol. 68, No. 3, pp. 505-513, 2024.

[17] R. M. KINDERMANN, M. J. ROY, R. MORANA, J. A. FRANCIS and P. B. PRANGNELL: 'Wire-arc directed energy deposition of Inconel 718: Effects of heat input and build interruptions on mechanical performance', *Additive Manufacturing*, Vol. 76, p. 103765, 2023.

[18] F. W. C. FARIAS, J. DA CRUZ PAYÃO FILHO and V. H. P. MORAES E OLIVEIRA: 'Prediction of the interpass temperature of a wire arc additive manufactured wall: FEM simulations and artificial neural network', *Additive Manufacturing*, Vol. 48, p. 102387, 2021.

[19] J. A. D.-D. LA PEÑA, P. A. LIMON-LEYVA, P. CORTES and K. CHOO: 'Modeling of Direct Energy Deposition for Wire Laser Additive Manufacturing', *J. of Materi. Eng. and Perform.*, vol. 34, no. 18, pp. 20648-20671, Sept. 2025, doi: 10.1007/s11665-025-10665-0.

[20] D. LÁZARO, A. ALONSO, M. LÁZARO and D. ALVEAR: 'A Simple Direct Method to Obtain Kinetic Parameters for Polymer Thermal Decomposition', *Applied Sciences*, vol. 11, no. 23, p. 11300, Nov. 2021, doi: 10.3390/app112311300.

[21] H. XIAO ET AL.: 'Influence of molten-pool cooling rate on solidification structure and mechanical property of laser additive manufactured Inconel 718', *Journal of Materials Research and Technology*, vol. 19, pp. 4404-4416, July 2022, doi: 10.1016/j.jmrt.2022.06.162.

[22] H. WANG, L. CAO, Y. LI, M. SCHNEIDER, E. DETEMPLE and G. EGGELER: 'Effect of cooling rate on the microstructure and mechanical properties of a low-carbon low-alloyed steel', *J. Mater. Sci.*, vol. 56, no. 18, pp. 11098-11113, June 2021, doi: 10.1007/s10853-021-05974-3.